Diagnosing satellite anomalies from time-varying similarity analyses in spectral imagery

Joseph Coughlin
Master Solutions
Colorado Springs, CO
joe.coughlin@mslco.com

ABSTRACT

Correctly determining satellite health and status is an important aspect in ascertaining satellite anomalies. Spectral data has often been proposed as having the potential to provide one part in the larger puzzle of determining satellite status. This paper presents the results of our study to clarify the utility of spectral data in ascertaining satellite anomalies, as compared to conventional broad-band imagery, using spectral similarity techniques.

This study focuses on the extraction of time varying signature distributions for non-resolved images using spectral similarity techniques. Analysis of the time varying distributions has potential to show the rough material similarities as a function of time without requiring a thorough material end-member extraction for each spectral image. We model time-varying multispectral and hyperspectral satellite signature images for different satellite models, configurations, and lighting conditions in the Thermal Infrared spectral region for a realistic sensor system. We analyze the resultant spectral signatures to determine spectral similarities and material distributions. By varying the model configurations we analyze the presence and distribution of different materials, reflectivity changes, rotation rates, and temporal changes to ascertain the effects of potential anomalies, such as incomplete or improper solar panel deployments.

To clarify the utility of spectral data, we compare the broad-band time variability in the signatures to the spectral similarity time variability. Our initial results indicate that spectral similarity derived from the spectral signatures can yield relevant information to determine satellite anomalies. This paper presents the results of our internal study to clarify the utility of spectral data in ascertaining satellite anomalies.

1. APPROACH

This study is an attempt to determine if spectral signature analyses can play a role in determining satellite status. For the purpose of this study we model two configurations of a hypothetical satellite. The first is a simple cubic body composed of typical satellite materials with three flat solar panels deployed on either side of the cube. The second configuration is the same cubic body with one solar panel deployed completely and the other solar panel partially deployed. The models used in the simulation are shown in Figure 1 and Figure 2, color coded with the different materials used in the models. The yellow is Kapton, the cyan is germanium, the green is mirrored surface, and the blue is the solar cell materials. The reflective and emissive spectral material properties are from an Air Force database.

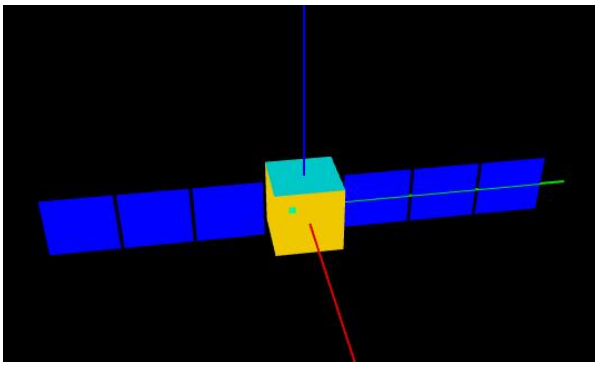

Figure 1. Satellite model with deployed solar panels

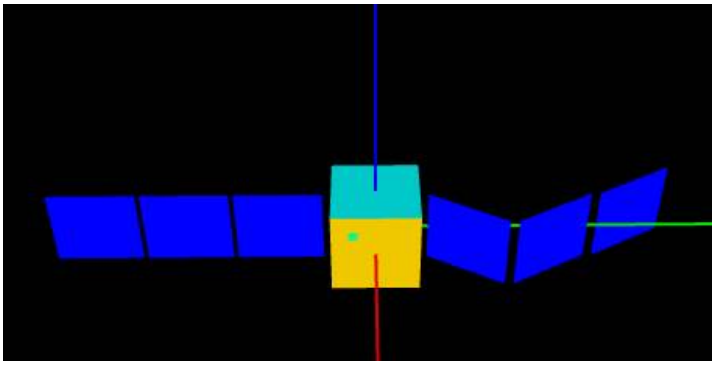

Figure 2. Satellite model with improperly deployed solar panel

The satellite is placed in a stable, non-tumbling configuration with the x-axis (red in the figure) pointed toward nadir. The z-axis (blue in the figure) is the direction of motion along the orbit. For the modeling effort, a notional sensor is positioned at 0 degrees latitude and 0 degrees longitude at an altitude of 2000 meters. A 1000 km circular orbit is chosen which passes within view of the site, while not going directly overhead, as shown in Figure 3. The orbit has a 45 degree inclination and the simulation goes from horizon to horizon.

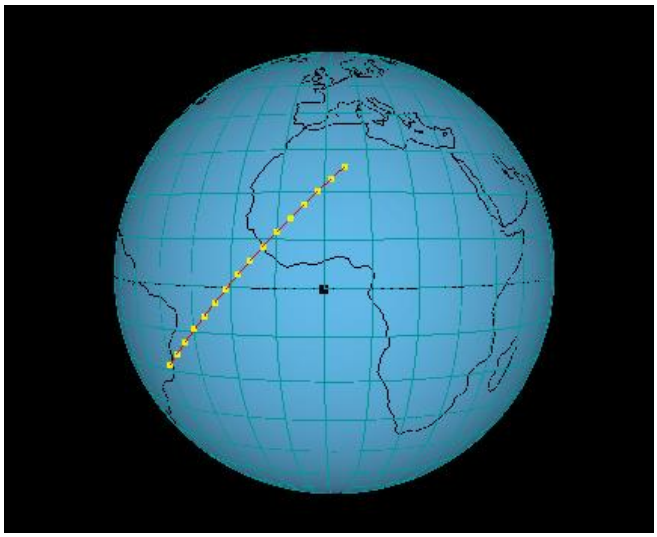

Figure 3. Satellite orbit and sensor position

Spectra are computed at 60 second increments along the orbital path. The spectral radiances are computed from 8-12 microns at 1 cm^{-1} and 2 cm^{-1}spectral resolution. In this spectral region the variations in the spectral signatures of the materials is not very large, so this analysis is likely to be a stressing case of using spectral similarity to differentiate signatures. The sensor zenith angle to the satellite as a function of simulation time is shown in Figure 4.

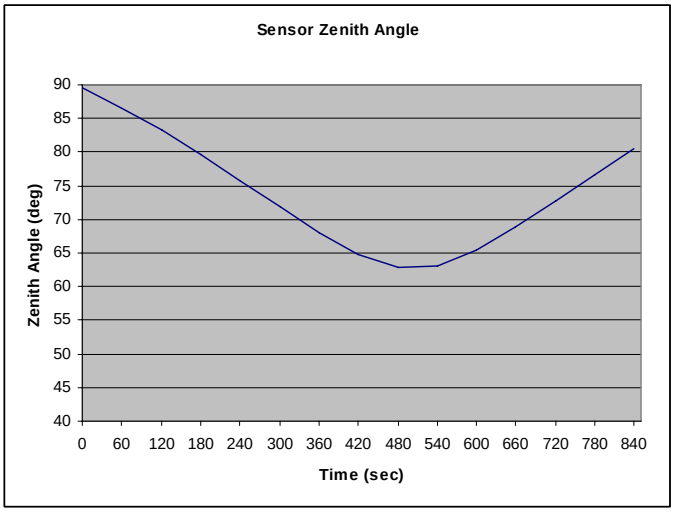

Figure 4. Sensor zenith angle

Since the computations are being performed in the thermal infrared, the atmospheric radiance can be an important contributor to the radiance and affects the ability to successfully analyze the spectral signatures. The airmass as a function of time is shown in Figure 5. At large airmasses, the signature of the satellite is lost in the radiance due to the atmosphere and large transmission loss.

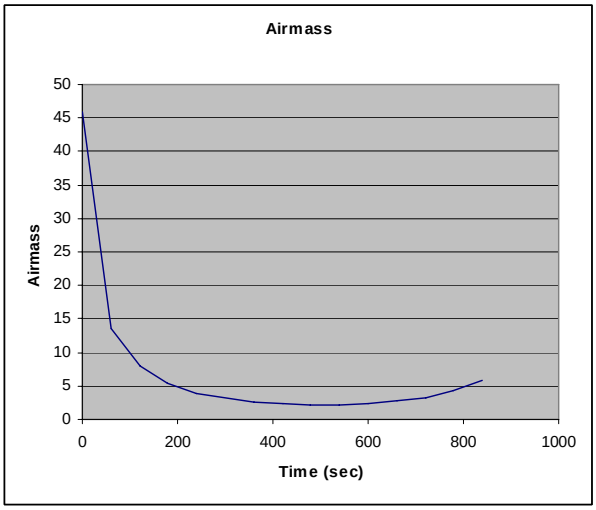

Figure 5. Airmass as a function of time

Computations are performed using the Master Solutions' Spectral Data Exploitation Workbench [1, 2]. The atmospheric radiative transfer calculations use the Emission Spectra (ES) [3] module, which is a line-by-line radiative transfer code. ES uses the Air Force HITRAN atmospheric line parameter database and a standard atmospheric model. More sophisticated models are available in the model, but were not used in this study. Atmospheric scattering was also ignored. The atmospheric radiance and transmission are calculated at each point along the orbit for the exact geometry of the sensor and satellite. The spectral radiance of the modeled "broken" satellite at the initial time step is shown in Figure 6.

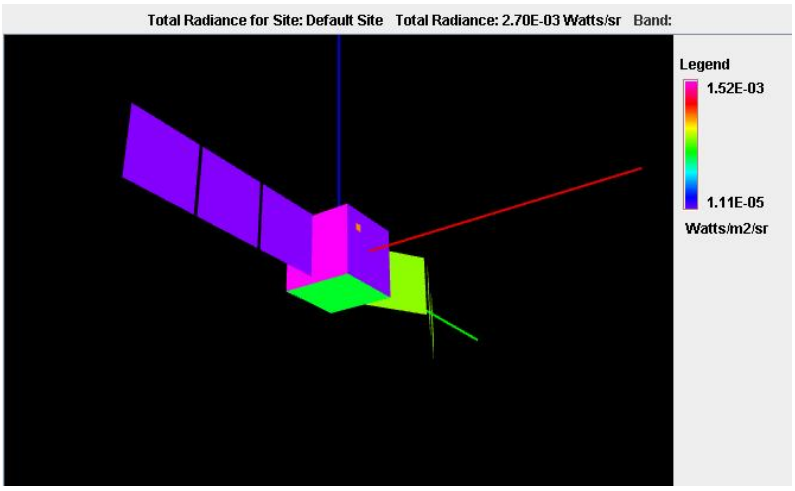

Figure 6. Initial radiance computation for "broken" satellite

This spectral image is then pixilated to simulate the response from a hypothetical sensor, as shown in Figure 7. Pixels are blended from the original image to yield a composite spectrum of the different materials. A background radiance spectrum is computed using only the atmosphere. This simulates the radiance in the image denoted by the black color and is used in the pixel blending. As will be seen, this background radiance can be a significant contribution to the radiance seen by the sensor in the thermal infrared.

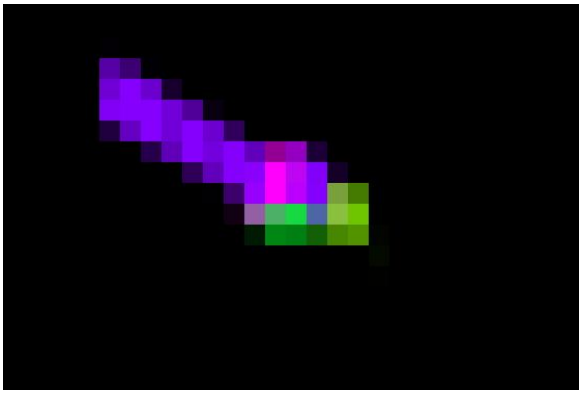

Figure 7. Pixilated image for "broken" satellite

The equivalent simulated pixilated image for the normal satellite is shown in Figure 8. For the purposes of this simulation, no additional noise is added, but future research can focus on the use of realistic sensor characteristics.

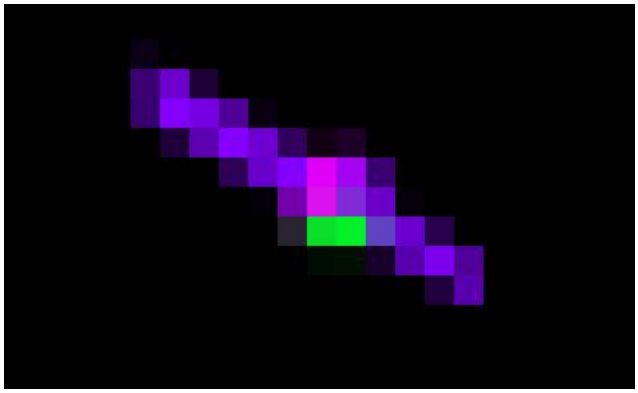

Figure 8. Pixilated radiance image for "normal" satellite

A quick comparison of the “normal” and “broken” images suggests that due to parts of the normal satellite being visible from the sensor, and consequently adding to the radiance signature, there is a perceptible difference. Keep in mind that in Figure 7 and Figure 8 the background radiance is not shown in the image.

2. RESULTS

For the satellite with the solar panel in the incorrect configuration, the “broken” satellite, we compute the total radiance as a function of time for the points along the orbit. These results are shown in Figure 9.

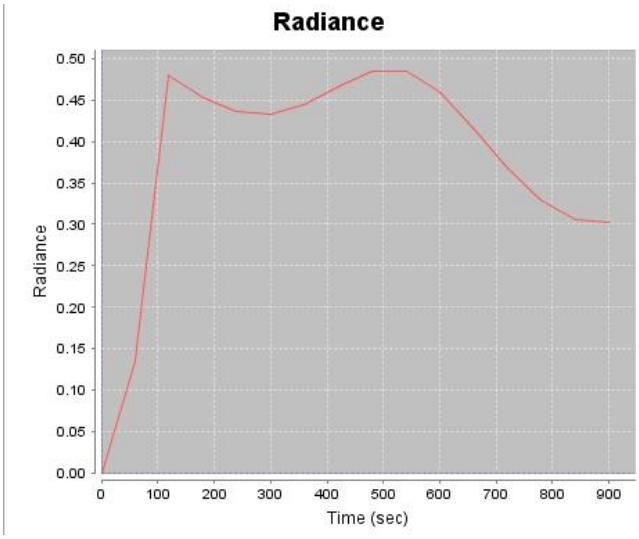

Figure 9. Total radiance as a function of time for the “broken” satellite

By comparison, the total radiance as a function of time for the “normal” satellite is shown in Figure 10.

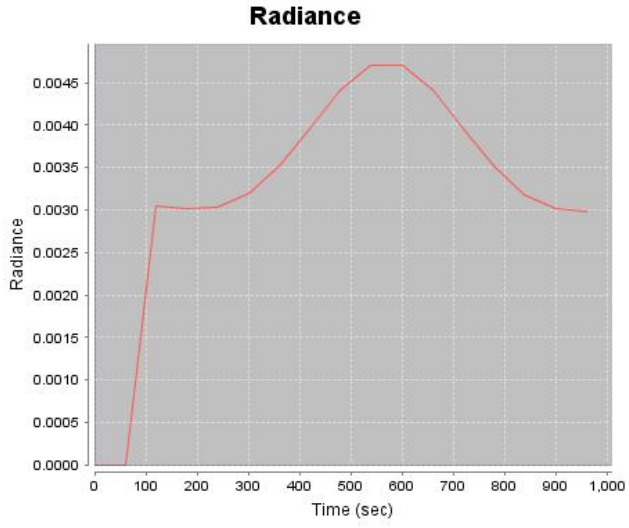

Figure 10. Total Radiance as a function of time for the “normal” satellite

Comparing the two figures shows that there are significant differences in the shapes of the total radiance curves for the “normal” and the “broken” satellites. When the atmospheric radiance is included in the computations, the resultant total radiance image for the “normal” satellite is shown in Figure 11 and the total radiance image for the “broken” satellite is shown in Figure 12 for t=240 seconds. A comparison of these radiance images shows that the

two satellites are clearly different. Note: for clarity in this presentation the images may be slightly rotated compared to one another. The radiance computations are performed for the same aspect angle as seen at the site.

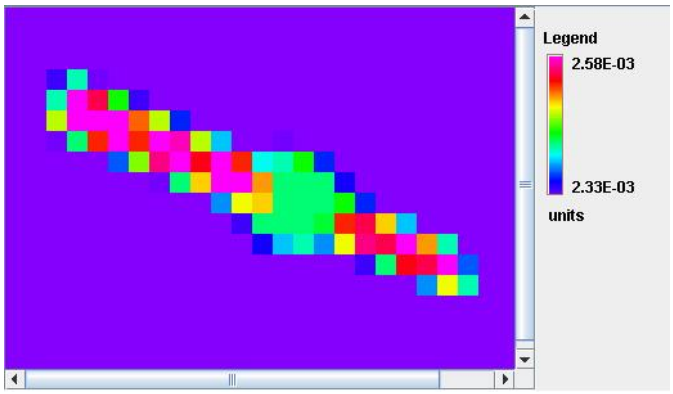

Figure 11. Total radiance image for "normal" at t=240 seconds

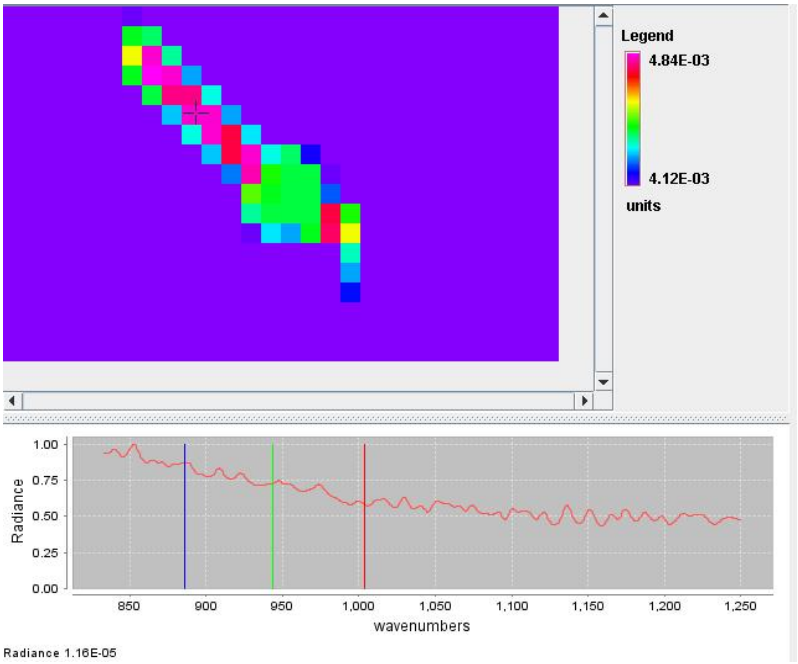

Figure 12. Total Radiance image for "broken" at t=240 seconds with selected spectrum

To determine if spectral similarity techniques have validity in diagnosing satellite anomalies, a simple Spectral Angle Mapper (SAM) algorithm is used to compare spectra within the image. Figure 12 shows the spectrum for the selected point that is used in the SAM calculation. The resultant image is gray-scaled to show how close the pixels match the selected spectrum. The selected pixel is shown by the cross-hairs in the image. To further show how close the pixels match the selection, an angular threshold is applied and all pixels that fall within that angular range are highlighted in red. Figure 13 shows the SAM results with the threshold applied on the "broken" satellite spectral image. Figure 14 shows the SAM results for the "normal" satellite applied with the same angular threshold as in the "broken" satellite case.

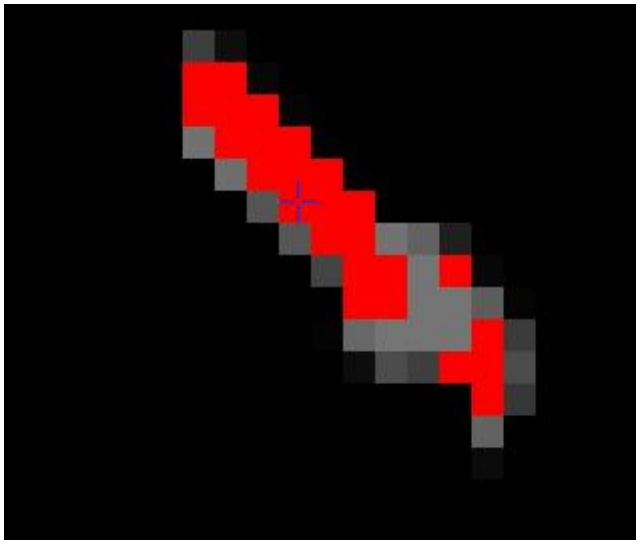

Figure 13. SAM results with threshold highlights on "broken" satellite

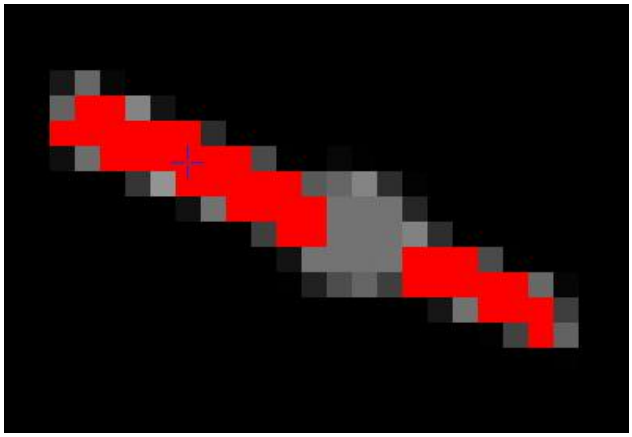

Figure 14. SAM results with threshold highlights on "normal" satellite

As time progresses through the orbit, the aspect angle of the satellite changes. Figure 15 shows the total radiance image for the "normal" satellite at t=480 seconds. At this time, the satellite has a near full viewing aspect as seen from the site.

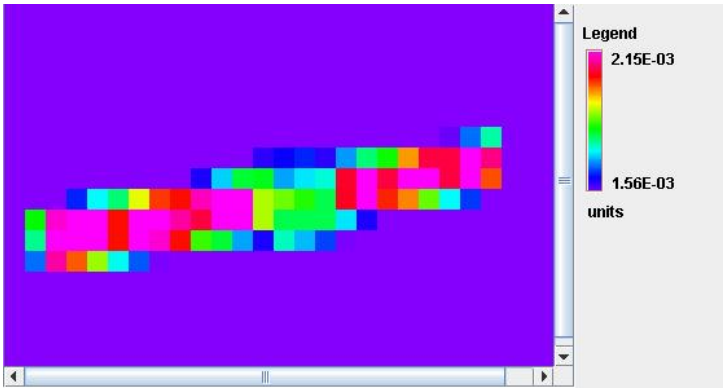

Figure 15. Total radiance image for "normal" satellite at t=480 seconds

Applying the same angular thresholds as in the previous SAM images yields the images in Figure 16 and Figure 17 for the “normal” and “broken” cases. As is clear from the images, the SAM results, as highlighted, are different for the “broken” satellite. The region where the solar panel is bent shows clearly by the lack of spectral similarity to the rest of the solar panel. It is also clear from the images that the solar material is differentiable from the Kapton insulation that surrounds the central region of the satellite.

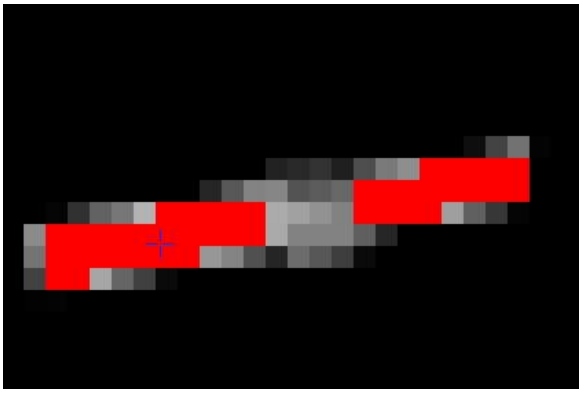

Figure 16. SAM results with threshold highlights for “normal” satellite

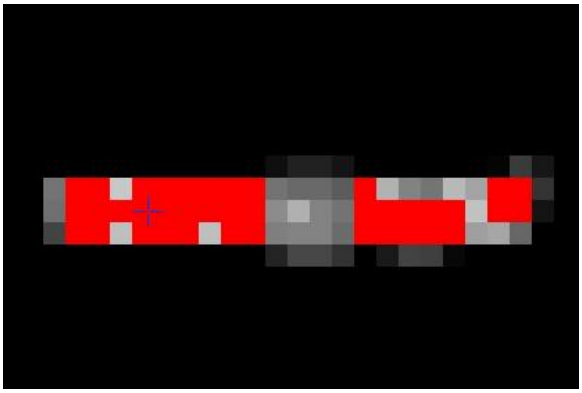

Figure 17. SAM results with threshold highlights for “broken” satellite

SAM results at other time steps within the orbit show the same results as presented here. Using the same SAM threshold value for all images taken along the orbit clearly shows that analyzing the time variability of the spectral signature shows the “broken” satellite is differentiable from the “normal” satellite.

3. CONCLUSIONS

This study has shown that there is a potential utility in using spectral similarity techniques to help ascertain satellite anomalies. Spectral data adds a dimension that can be exploited by even simple techniques to yield additional insights. Utilizing even a simple technique such as a Spectral Angle Mapper algorithm with threshold highlighting (spectral alarming) on spectral imagery can show an operator more information than is available via broad band imagery. Other spectral regions where there is a larger variability in the spectral signatures due to the different materials can be expected to yield similar, or even better results than shown here. More sophisticated techniques which extract information on materials within a pixel may also yield improved results.

Although this study was performed to determine if these techniques can be used to diagnose satellite anomalies, these techniques can be used in other operational concepts. Similar signature analyses could be performed on satellites where it is desirable to monitor the configuration over time. For example, observations of solar panel deployments could be made to verify proper operations. Observations over time could be used to evaluate normal health signatures. Analyses of the satellite signatures could evaluate launch profiles, satellite dispensing, and normal operations.

4. REFERENCES

1. Coughlin, J., Analysis of Atmospheric Impact on the Evaluation of Hyperspectral Imagery, Advanced Maui Optical and Space Surveillance Technologies Conference, Maui, HI, September 2006
2. Coughlin, J., Emission Spectra: A Multi-Purpose Radiative Transfer Environment for Hyperspectral Data Modeling and Exploitation, Proceedings International Symposium on Spectral Sensing Research, Maui, HI, November 1992
3. Coughlin, J., ES: A Fast Line Code, Proceedings Electro-Optical Aerial Targeting Models Users Meeting, Dayton, OH, June 1990
4. Chang, Chien-I, *Hyperspectral Imaging: Techniques for Spectral Detection and Classification*, Klewer Academic/Plenum Publishers, New York, 2003.